Stabilization of higher-order high resolution schemes for the compressible Navier-Stokes equations

H. Daiguji
Emeritus Professor, Tohoku University, Sendai, Japan
X. Yuan
Department of Thermal Engineering, Tsinghua University, Beijing, China, and
S. Yamamoto
Department of Aeronautics and Space Engineering, Tohoku University, Sendai, Japan

Introduction

The shock wave which is a discontinuity in the high-speed compressible flow can be captured sufficiently by using the usual second-order high resolution TVD schemes, for example the Chakravarthy-Osher TVD scheme[1] and the Lax-Wendroff TVD scheme[2,3]. However, it is difficult to simulate sharply weak discontinuities like a slip surface or contact surface by such high-resolution schemes. The reason is that a slip line emanates from a junction of shock waves, is smeared mainly by the numerical diffusion on the downstream side of the junction and does not return to the original sharp slip line again. Therefore, in the simulation of the weak discontinuity, it is necessary to use the scheme which has a very small truncation error, while for capturing the shock wave the conservative character of the scheme plays an important role.

We have recently proposed the fourth(fifth)-order high resolution TVD schemes[4,5] which are higher-order versions of the third-order Chakravarthy-Osher scheme, and by using these schemes have been able to simulate the slip lines fairly well. In the present paper, some numerical schemes for the compressible flows recently developed in our laboratory will be described, in particular a stabilization process for the fourth(fifth)-order schemes. In this fourth-order scheme, all the slopes $\Delta u_{j+1/2}$ in the correction terms of the third-order Chakravarthy-Osher scheme, which are added to the first-order upstream-difference scheme to modify the third order, are simply replaced by

$$Du_{j+1/2} \equiv \Delta u_{j+1/2} - \frac{1}{6}\Delta^3 u_{j+1/2}$$

where $\Delta^3 u$ is the third-order difference of u. Therefore, the existing programmes

International Journal of Numerical Methods for Heat & Fluid Flow
Vol. 7 No. 2/3, 1997, pp. 250-274.

of the Chakravarthy-Osher scheme can be rewritten quite easily into programmes of the present fourth-order scheme, and computational efforts are barely increased by this rewriting.

If the function $u(x)$ itself and the derivatives $u'(x)$, $u''(x)$, … are sufficiently smooth, and the Taylor series of u_j converges well, then the solution of the transport equation can be computed stably by an appropriate higher-order scheme using a sufficiently smooth fine mesh. However, in the practical calculation, the slopes $\Delta u_{j+1/2}$ do not always vary so smoothly and even contain some numerical disturbances. Therefore, the solution becomes more unstable by using the higher-order scheme, because the modified slopes $Du_{j+1/2}$ in general tend to contain magnified disturbances. Key points of the proposed method are that the third-order differences are expressed as

$$\Delta^3 u_{j+1/2} = \Delta^2 u_{j+1} - \Delta^2 u_j$$

and that the values of $\Delta^3 u_{j+1/2}$ are restricted by operating the minmod function to the curvatures $\Delta^2 u_j$. In the Chakravarthy-Osher scheme, the values of the second(third)-order correction terms are restricted by the limiter function in order to prevent the occurrence of new extremum points. In the present scheme, in addition to this restriction, the values of the fourth(fifth)-order correction terms are restricted by another limiter function in order to suppress the occurrence of new inflection points.

In the following section, fundamental equations of the compressible turbulent flows and an outline of our schemes will be described. The next section is devoted to stabilization of the fourth(fifth)-order TVD scheme. Then, the recently developed efficient algorithms for the delta-form implicit schemes are briefly explained. Finally, some numerical results of steady and unsteady transonic flows through a turbine cascade are shown.

Fundamental equations and numerical schemes

The governing equations of compressible turbulent flows used in the practical computation are the Reynolds-averaged compressible Navier-Stokes equations and some turbulence model. Here the N-S equations of volume flux J**U** in general curvilinear coordinates[6] and the low Reynolds number k-ε turbulence model modified by Chien[7] are used. The N-S equations are

$$B\left[\frac{\partial \hat{q}}{\partial t} + \frac{\partial \hat{F}_i}{\partial \xi_i} + \hat{D} + \hat{g}\right] = \frac{\partial \tilde{q}}{\partial t} + \frac{\partial \tilde{F}_i}{\partial \xi_i} + \tilde{R} + \tilde{D} + \tilde{g} = 0, \qquad (1)$$

where the dependent variable vectors $\hat{q}$ and $\tilde{q}$, the flux vectors $\hat{F}_i$ and $\tilde{F}_i$, the diffusion term $\hat{D}$, and the linear transformation matrix B are

$$\tilde{q} = J\begin{bmatrix} \rho \\ \rho u \\ \rho v \\ \rho w \\ \rho E \end{bmatrix}, \quad \hat{F}_i = J\begin{bmatrix} \rho U_i \\ \rho u U_i + \xi_{i,1} p \\ \rho v U_i + \xi_{i,2} p \\ \rho w U_i + \xi_{i,3} p \\ \rho H U_i \end{bmatrix}, \quad (i = 1,2,3)$$

$$\tilde{q} = J\begin{bmatrix} \rho \\ \rho U \\ \rho V \\ \rho W \\ \rho E \end{bmatrix}, \quad \hat{F}_i = J\begin{bmatrix} \rho U_i \\ \rho U U_i + g_{i1} p \\ \rho V U_i + g_{i2} p \\ \rho W U_i + g_{i3} p \\ \rho H U_i \end{bmatrix}, \quad (i = 1,2,3)$$

$$\hat{D} = -\frac{\partial}{\partial \xi_i} J \xi_{i,j} \begin{bmatrix} 0 \\ \tau_{1j} \\ \tau_{2j} \\ \tau_{3j} \\ \tau_{jk} u_k + \kappa T_{,j} \end{bmatrix}, \quad B = \begin{bmatrix} 1 & 0 & 0 & 0 & 0 \\ 0 & \xi_{1,1} & \xi_{1,2} & \xi_{1,3} & 0 \\ 0 & \xi_{2,1} & \xi_{2,2} & \xi_{2,3} & 0 \\ 0 & \xi_{3,1} & \xi_{3,2} & \xi_{3,3} & 0 \\ 0 & 0 & 0 & 0 & 1 \end{bmatrix} \tag{2}$$

$\tilde{R}$ is an additional term introduced to express the flux term in conservative form, $\hat{g}$ and $\tilde{g}$ are the force terms, U, V and W are the contravariant velocities, E is the stagnation internal energy and H is the stagnation enthalpy. $J = \partial(x_1, x_2, x_3)/\partial(\xi_1, \xi_2, \xi_3)$, $\xi_{i,j} = \partial\xi_i/\partial x_j$ and $g_{ij} = \nabla\xi_i \cdot \nabla\xi_j$. The static pressure and the static temperature can be obtained from the equation of state

$$p = \rho RT = (\gamma - 1)\rho(E - \frac{1}{2}u_i u_i). \tag{3}$$

The Cartesian components of the viscous and Reynolds stress tensor τ_{ij} and the heat flux $\kappa T_{,j}$ for the eddy viscosity turbulence model are given by

$$\begin{aligned} \tau_{ij} &= (\mu + \mu_t)(u_{i,j} + u_{j,i} - \frac{2}{3}\delta_{ij}u_{k,k}) - \frac{2}{3}\delta_{ij}\rho k, && (i,j = 1,2,3) \\ \kappa T_{,j} &= \frac{1}{\gamma - 1}\left(\frac{\mu}{Pr} + \frac{\mu_t}{Pr_t}\right)c^2_{,j} && (j = 1,2,3) \end{aligned} \tag{4}$$

where Pr and Pr_t are the usual and turbulent Prandtl numbers.

The eddy viscosity for the low Reynolds number k-ε model is expressed as

$$\mu_t = C_\mu f_\mu \rho k^2/\varepsilon, \tag{5}$$

and the turbulence kinetic energy k and the dissipation rate ε are obtained by solving the transport equations

$$\frac{\partial \hat{q}_t}{\partial t} + \frac{\partial \hat{F}_{ti}}{\partial \xi_i} + \hat{D}_t + \hat{g}_t = 0 \tag{6}$$

where

$$\hat{q}_t = J\begin{bmatrix} \rho k \\ \rho \varepsilon \end{bmatrix}, \qquad \hat{F}_{ti} = \begin{bmatrix} \rho k U_i \\ \rho \varepsilon U_i \end{bmatrix}, \qquad (i = 1, 2, 3)$$

$$\hat{D}_t = -\frac{\partial}{\partial \xi_i} J g_{ij} \begin{bmatrix} \left(\mu + \dfrac{\mu_t}{Pr_k}\right)\dfrac{\partial k}{\partial \xi_j} \\ \left(\mu + \dfrac{\mu_t}{Pr_\varepsilon}\right)\dfrac{\partial \varepsilon}{\partial \xi_j} \end{bmatrix},$$

$$\hat{g}_t = -J \begin{bmatrix} P - \rho\varepsilon - \dfrac{2\mu k}{d^2} \\ \dfrac{\varepsilon}{k}\left(C_1 f_1 P - C_2 f_2 \rho\varepsilon - \dfrac{C_3 f_3 2\mu k}{d^2}\right) \end{bmatrix}. \tag{7}$$

$P = \rho\overline{u_i' u_j'}\, u_{i,j}$ is the production, d is the distance from the solid wall and C_μ, C_i, f_μ and f_i are the empirical constants and functions which can be found in [7]. The turbulence transport equations of (6) are usually solved simultaneously with the Reynolds averaged flow equations of (1).

The flux vector $\hat{F}_i$ can be linearized and diagonalized in a way similar to the flux vector $\hat{F}_i$.

$$\begin{aligned} \hat{F}_i &= \hat{A}_i \hat{q}, \quad \hat{A}_i = \hat{R}_i \hat{\Lambda}_i \hat{L}_i, \\ \tilde{F}_i &= \tilde{A}_i \tilde{q}, \quad \tilde{A}_i = \tilde{R}_i \tilde{\Lambda}_i \tilde{L}_i \end{aligned} \qquad (i = 1, 2, 3) \tag{8}$$

where $\hat{L}_i \hat{R}_i = \tilde{L}_i \tilde{R}_i = I$, $\hat{\Lambda}_i = \tilde{\Lambda}_i$.

$$\tilde{A}_i = \begin{bmatrix} 0 & \delta_{1i} & \delta_{2i} & \delta_{3i} & 0 \\ -UU_i + \phi^2 g_{1i} & U_i + \delta_{1i}U - \alpha_1 g_{1i} & \delta_{2i}U - \alpha_2 g_{2i} & \delta_{3i}U - \alpha_3 g_{1i} & \tilde{\gamma} g_{1i} \\ -VU_i + \phi^2 g_{2i} & \delta_{1i}V - \alpha_1 g_{2i} & U_i + \delta_{2i}V - \alpha_2 g_{2i} & \delta_{3i}V - \alpha_3 g_{2i} & \tilde{\gamma} g_{2i} \\ -WU_i + \phi^2 g_{3i} & \delta_{1i}W - \alpha_1 g_{3i} & \delta_{2i}W - \alpha_2 g_{3i} & U_i + \delta_{3i}W - \alpha_3 g_{3i} & \tilde{\gamma} g_{3i} \\ -HU_i + \phi^2 U_i & \delta_{1i}H - \alpha_1 U_i & \delta_{2i}H - \alpha_2 U_i & \delta_{3i}H - \alpha_3 U_i & \gamma U_i \end{bmatrix},$$

$$\tilde{R}_i = \begin{bmatrix} 1 & 0 & 0 & 0 & 0 \\ U & 1 & 0 & 0 & 0 \\ V & 0 & 1 & 0 & 0 \\ W & 0 & 0 & 1 & 0 \\ \phi^2/\tilde{\gamma} & \alpha_1/\tilde{\gamma} & \alpha_2/\tilde{\gamma} & \alpha_3/\tilde{\gamma} & 1/\tilde{\gamma} \end{bmatrix}$$

$$\times \begin{bmatrix} 1 & \delta_{1i}/2c\sqrt{g_{11}} & \delta_{2i}/2c\sqrt{g_{22}} & \delta_{3i}/2c\sqrt{g_{33}} & 1/2c\sqrt{g_{ii}} \\ 0 & 1-\delta_{1i}/2 & \delta_{2i}g_{12}/2g_{22} & \delta_{3i}g_{13}/2g_{33} & -g_{1i}/2g_{ii} \\ 0 & \delta_{1i}g_{21}/2g_{11} & 1-\delta_{2i}/2 & \delta_{3i}g_{23}/2g_{33} & -g_{2i}/2g_{ii} \\ 0 & \delta_{1i}g_{31}/2g_{11} & \delta_{2i}g_{32}/2g_{22} & 1-\delta_{3i}/2 & -g_{3i}/2g_{ii} \\ 0 & \delta_{1i}c/2\sqrt{g_{11}} & \delta_{2i}c/2\sqrt{g_{22}} & \delta_{3i}c/2\sqrt{g_{33}} & c/2\sqrt{g_{ii}} \end{bmatrix},$$

$$\tilde{\Lambda}_i = \begin{bmatrix} U_i & 0 & 0 & 0 & 0 \\ 0 & U_i+\delta_{1i}c\sqrt{g_{11}} & 0 & 0 & 0 \\ 0 & 0 & U_i+\delta_{2i}c\sqrt{g_{22}} & 0 & 0 \\ 0 & 0 & 0 & U_i+\delta_{3i}c\sqrt{g_{33}} & 0 \\ 0 & 0 & 0 & 0 & U_i-c\sqrt{g_{ii}} \end{bmatrix},$$

$$\tilde{L}_i = \begin{bmatrix} 1 & 0 & 0 & 0 & -1/c^2 \\ 0 & 1 & -\delta_{2i}g_{12}/g_{22} & -\delta_{3i}g_{13}/g_{33} & \delta_{1i}\sqrt{g_{11}}/c \\ 0 & -\delta_{1i}g_{21}/g_{11} & 1 & -\delta_{3i}g_{23}/g_{33} & \delta_{2i}\sqrt{g_{22}}/c \\ 0 & -\delta_{1i}g_{31}/g_{11} & -\delta_{2i}g_{32}/g_{22} & 1 & \delta_{3i}\sqrt{g_{33}}/c \\ 0 & \delta_{1i} & \delta_{2i} & \delta_{3i} & -\sqrt{g_{jj}}/c \end{bmatrix}$$

$$\times \begin{bmatrix} 1 & 0 & 0 & 0 & 0 \\ -U & 1 & 0 & 0 & 0 \\ -V & 0 & 1 & 0 & 0 \\ -W & 0 & 0 & 1 & 0 \\ \phi^2 & -\alpha_1 & -\alpha_2 & -\alpha_3 & \tilde{\gamma} \end{bmatrix}, \qquad (i = 1, 2, 3) \tag{9}$$

$\phi^2 = \frac{1}{2}\tilde{\gamma}\boldsymbol{u}^2$, $\alpha_j = \tilde{\gamma}u_k\partial x_k/\partial\xi_j$ and $\tilde{\gamma} = \gamma - 1$.

In the calculation of the steady flows, the efficient time-marching method by the delta-form implicit schemes is used. Applying the trapezoidal law to the fundamental equations (1) and (6), rewriting into the delta-form and using the linearization of (8), we obtain

$$\left(I + \Delta t\,\theta\frac{\partial}{\partial\xi_i}\tilde{A}_i^n\right)\Delta\tilde{q}^n = RHS^n \tag{10}$$

where

$$\tilde{q}^{n+1} = \tilde{q}^n + \Delta\tilde{q}^n ,$$
$$RHS = -\Delta t\, B \left(\frac{\partial \hat{F}_i}{\partial \xi_i} + \hat{D} + \hat{g} \right) . \tag{11}$$

Similarly, in the calculation of the unsteady flows, applying the second-order Crank-Nicholson method to (1) and (6) and further using the Newton iteration to make the solution converge at each time step, we obtain the equation of delta-form implicit scheme

$$(I + \Delta t\, \theta \frac{\partial}{\partial \xi_i} \tilde{A}_i^n) \Delta\tilde{q}^{(m)} = -(\tilde{q}^{(m-1)} - \tilde{q}^n) + \frac{1}{2}(RHS^n + RHS^{(m-1)}) \tag{12}$$

where

$$\tilde{q}^{(m)} = \tilde{q}^{(m-1)} + \Delta\tilde{q}^{(m)} ,$$

$\tilde{q}^{(0)} = \tilde{q}^n$, $\tilde{q}^{(m)}$ ($m \geq 1$) is the m-th approximation of $\tilde{q}^{n+1}$. The solution usually converges within three to five time iterations.

The right-hand side of (10) or (12) means residuals of the fundamental equations. The accuracy of the solution only depends on *RHS*. Therefore, the value of *RHS* must be calculated exactly using a higher-order upstream-difference scheme in the somewhat simple expression of the left-hand side of (1). $\Delta\tilde{q}^n$ and $\Delta\tilde{q}^{(m)}$ are the corrections of $\tilde{q}$ and $\tilde{q}^{n+1}$, respectively. Since the accuracy is independent of the left-hand-side operator, the left-hand side is treated approximately using the simplest and most stable first-order upstream-difference scheme. θ is usually taken as 1, and then these schemes become TVD stable even for the large value of Δt.

Higher-order TVD schemes

The first derivatives in (11) are approximated by the higher-order finite-differences written in the conservative form

$$(f_{,x})_\ell = \frac{1}{\Delta x}(h_{\ell+1/2} - h_{\ell-1/2}) \tag{13}$$

where h is the numerical flux function of f, and for the first-order upstream-difference scheme it becomes as

$$h_{\ell+1/2} = h^{(1)}_{\ell+1/2} \equiv \frac{1}{2}(f_\ell + f_{\ell+1}) - \frac{1}{2}(\Delta f^+_{\ell+1/2} - \Delta f^-_{\ell+1/2}) . \tag{14}$$

And for the second(third)-order Chakravarthy-Osher TVD scheme the flux function is

$$h_{\ell+1/2} = h^{(1)}_{\ell+1/2} + \frac{1-\kappa}{4}\Delta\tilde{f}^{+}_{\ell-1/2} + \frac{1+\kappa}{4}\Delta\tilde{f}^{+}_{\ell+1/2} - \frac{1-\kappa}{4}\Delta\tilde{f}^{-}_{\ell+3/2} - \frac{1+\kappa}{4}\Delta\tilde{f}^{-}_{\ell+1/2} \tag{15}$$

where

$$\begin{aligned} \Delta\tilde{f}^{\pm}_{j+1/2} &= \mathrm{minmod}(\Delta f^{\pm}_{j+1/2},\ b\Delta f^{\pm}_{j-1/2}), \qquad (j = \ell,\ \ell+1) \\ \Delta\tilde{\tilde{f}}^{\pm}_{j+1/2} &= \mathrm{minmod}(\Delta f^{\pm}_{j+1/2},\ b\Delta f^{\pm}_{j+3/2}), \qquad (j = \ell-1,\ \ell) \end{aligned} \tag{16}$$

minmod (x,y) = sign (x) max $[0, \min\{|x|, \mathrm{sign}\,(x)\,y\}]$.

Let us consider the linearization of flux $\Delta f = a\Delta u$, where $a = \partial f/\partial u$ is the phase velocity. In order to obtain the reasonable numerical flux from (13) to (16), the upstreaming must be made using the common phase velocity $a^{\pm}_{\ell+1/2}$ as

$$\begin{aligned} \Delta f^{\pm}_{j+1/2} &= a^{\pm}_{\ell+1/2}\Delta u_{j+1/2}, \\ \Delta u_{j+1/2} &= u_{j+1} - u_j, \qquad (j = \ell-1,\ \ell,\ \ell+1) \end{aligned} \tag{17}$$

or according to the sign of $a^{\pm}_{\ell+1/2}$ as

$$\begin{aligned} \Delta f^{\pm}_{j+1/2} &= |\mathrm{sign}(a^{\pm}_{\ell+1/2})|\,\Delta f_{j+1/2}, \quad \Delta f_{j+1/2} = f_{j+1} - f_j, \\ \mathrm{sign}(a^{+}) &= \begin{cases} 1 & (a > 0) \\ 0 & (a \le 0) \end{cases}, \qquad \mathrm{sign}(a^{-}) = \begin{cases} 0 & (a \ge 0) \\ -1 & (a < 0) \end{cases}, \end{aligned} \tag{18}$$

$a^{\pm} = (a \pm |a|)/2$.

If no slope $\Delta f_{j+1/2}$ is restricted by the limiter, then the truncation errors of (15) are

$$(f_{,x})_\ell - \frac{1}{\Delta x}(h_{\ell+1/2} - h_{\ell-1/2}) = -\frac{1}{12}(3\kappa - 1)\Delta x^2 (f_{xxx})_\ell + \mathrm{O}(\Delta x^3).$$

Therefore, the C-O scheme is third order only for $\kappa = 1/3$. The flux function of the fourth(fifth)-order upstream-difference scheme is

$$\begin{aligned} h_{\ell+1/2} = h^{(1)}_{\ell+1/2} &+ \frac{1}{6}\Delta f^{+}_{\ell-1/2} - \frac{1-\phi}{24}\Delta^3 f^{+}_{\ell-1/2} \\ &+ \frac{1}{3}\Delta f^{+}_{\ell+1/2} - \frac{1+\phi}{24}\Delta^3 f^{+}_{\ell+1/2} \\ &- \frac{1}{6}\Delta f^{-}_{\ell+3/2} + \frac{1-\phi}{24}\Delta^3 f^{-}_{\ell+3/2} \\ &- \frac{1}{3}\Delta f^{-}_{\ell+1/2} + \frac{1+\phi}{24}\Delta^3 f^{-}_{\ell+1/2} \end{aligned} \tag{19}$$

where

$$\begin{aligned}\Delta^3 f_{j+1/2} &= \Delta f_{j-1/2} - 2\Delta f_{j+1/2} + \Delta f_{j+3/2} \\ &= \Delta^2 f_{j+1} - \Delta^2 f_j . \qquad (j = \ell - 1,\ \ell,\ \ell + 1)\end{aligned} \tag{20}$$

This flux function is a sum of the flux function of third-order C-O scheme and the fourth(fifth)-order corrections which are the third-order differences. The truncation errors of (19) are

$$(f_{,x})_\ell - \frac{1}{\Delta x}(h_{\ell+1/2} - h_{\ell-1/2}) = -\frac{4}{15}(1 - 5\phi)\Delta x^4 (f_{xxxxx})_\ell + \mathrm{O}(\Delta x^5)$$

Therefore, this scheme is fifth order only for $\phi = 1/5$, but we can obtain similar excellent results for ϕ close to 1/5.

The TVD schemes of (19) are considered next. Referring to the TVD scheme of (15), we find that the TVD condition is at once satisfied by the equation

$$(f_{,x})_\ell - \frac{1}{\Delta x}(h_{\ell+1/2} - h_{\ell-1/2}) = -\frac{4}{15}(1 - 5\phi)\Delta x^4 (f_{xxxxx})_\ell + \mathrm{O}(\Delta x^5) . \tag{21}$$

where

$$\begin{aligned}\tilde{Df}^{\pm}_{j+1/2} &= \mathrm{minmod}(Df^{\pm}_{j+1/2},\ bDf^{\pm}_{j-1/2}) , \qquad (j = \ell,\ \ell + 1) \\ \tilde{Df}^{\pm}_{j+1/2} &= \mathrm{minmod}(Df^{\pm}_{j-1/2},\ bDf^{\pm}_{j+3/2}) . \qquad (j = \ell - 1,\ \ell)\end{aligned} \tag{22}$$

In order to modify the scheme in fifth order, $Df_{j+1/2}$ must be taken as

$$\begin{aligned}Df^{+}_{\ell-1/2} &= \Delta f^{+}_{\ell-1/2} - \frac{1}{5}\Delta^3 \bar{f}^{+}_{\ell-1/2} , \\ Df^{\pm}_{\ell+1/2} &= \Delta f^{\pm}_{\ell+1/2} - \frac{3}{20}\Delta^3 \bar{f}^{\pm}_{\ell+1/2} , \\ Df^{-}_{\ell+3/2} &= \Delta f^{-}_{\ell+3/2} - \frac{1}{5}\Delta^3 \bar{f}^{-}_{\ell+3/2} .\end{aligned} \tag{23}$$

On the other hand, if $\phi = 1/3$, then $Df_{j+1/2}$ can be expressed in the unified form

$$Df^{\pm}_{j+1/2} = \Delta f^{\pm}_{j+1/2} - \frac{1}{6}\Delta^3 \bar{f}^{\pm}_{j+1/2} . \qquad (j = \ell - 1,\ \ell,\ \ell + 1) \tag{24}$$

Then, the existing computer programmes for the Chakravarthy-Osher TVD scheme can be rewritten very easily into programmes for this fourth-order scheme.

In the previous method[4], in order to satisfy the TVD condition completely, the condition $Df = \Delta f$, that is, $\Delta^3 f = 0$ was imposed near the extremum point of f. From this condition, the fifth- and fourth-order correction terms in (23) and (24) were restricted as

$$\Delta^3 \bar{f}^{\pm}_{j+1/2} = \Delta \bar{f}^{\pm}_{j-1/2} - 2\Delta \bar{f}^{\pm}_{j+1/2} + \Delta \bar{f}^{\pm}_{j+3/2} \qquad (j = \ell - 1,\ \ell,\ \ell + 1) \tag{25}$$

where

$$\begin{aligned}
\Delta\bar{f}^{\pm}_{j-1/2} &= \text{minmod}(\Delta f^{\pm}_{j-1/2},\ b_1\Delta f^{\pm}_{j+1/2},\ b_1\Delta f^{\pm}_{j+3/2}),\\
\Delta\bar{f}^{\pm}_{j+1/2} &= \text{minmod}(\Delta f^{\pm}_{j+1/2},\ b_1\Delta f^{\pm}_{j+3/2},\ b_1\Delta f^{\pm}_{j-1/2}),\\
\Delta\bar{f}^{\pm}_{j+3/2} &= \text{minmod}(\Delta f^{\pm}_{j+3/2},\ b_1\Delta f^{\pm}_{j-1/2},\ b_1\Delta f^{\pm}_{j+1/2}),
\end{aligned} \tag{26}$$

$\text{minmod}(x, y, z) = \text{sign}(x)\max[0, \min\{|x|, \text{sign}(x)\,y, \text{sign}(x)\,z\}]$.

The value of the parameter b_1 is usually taken as 2.

In the Chakravarthy-Osher TVD scheme of (15), the second(third)-order correction terms are restricted by operating the minmod function to the slopes $\Delta f_{j+1/2}$ to prevent the occurrence of new extremums of f caused by these correction terms. From the condition that $h_{\ell+1/2}$ does not take a peak value of f, the parameter b in (16) must be taken $1 < b \le (3-\kappa)/(1-\kappa)$. The values of $Df_{j+1/2}$ of (23) and (24) contain in general amplified disturbances compared with $\Delta f_{j+1/2}$ as shown in Figure 1. The fourth(fifth)-order correction terms in (19) of course raises the accuracy of solution especially containing the weak discontinuity, but often unstabilizes the solution. Therefore, in the present method these correction terms are restricted by operating another minmod function to the curvatures $\Delta^2 f_j$, in order to suppress the occurrence of new extremums of Δf, that is, new inflection points of f.

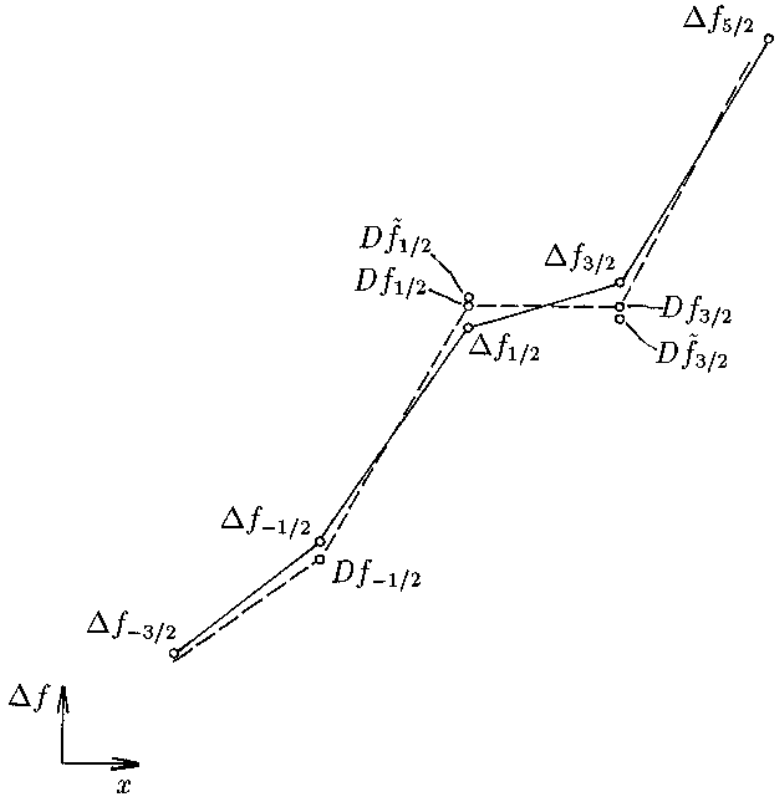

Figure 1.
Typical distributions of slopes $\Delta f_{j+1/2}$, $D\tilde{f}_{j+1/2} \equiv \Delta f_{j+1/2} - (\Delta^2 f_{j+1} - \Delta^2 f_j)/6$ and $Df_{j+1/2} \equiv \Delta f_{j+1/2} - [\text{minmod}(\Delta^2 f_{j+1/2}, 4\Delta^2 f_j) - \text{minmod}(\Delta^2 f_j, 4\Delta^2 f_{j+1})]/6$

$$\Delta^3 \tilde{f}^{\pm}_{j+1/2} = \Delta^2 \tilde{f}^{\pm}_{j+1} - \Delta^2 \tilde{\tilde{f}}^{\pm}_{j} \qquad (j = \ell - 1, \ell, \ell + 1) \quad (27)$$

where

$$\begin{aligned} \Delta^2 \tilde{f}^{\pm}_{k} &= \text{minmod}(\Delta^2 f^{\pm}_{k},\ b_2 \Delta^2 f^{\pm}_{k-1}), \\ \Delta^2 \tilde{\tilde{f}}^{\pm}_{k} &= \text{minmod}(\Delta^2 f^{\pm}_{k},\ b_2 \Delta^2 f^{\pm}_{k+1}), \\ \Delta^2 f_k &= \Delta f_{k+1/2} - \Delta f_{k-1/2}. \end{aligned} \quad (28)$$

The range of parameter b_2 is determined so that $Df_{j+1/2}$ does not take a peak value. We first consider the case that $|\Delta^2 f_j| > b_2 |\Delta^2 f_{j+1}|$. Then

$$Df_{j+1/2} = \Delta f_{j+1/2} + \frac{1}{6}(b_2 - 1)\Delta^2 f_{j+1}.$$

Since the value of $Df_{j+1/2}$ should not exceed the mean value of $\Delta f_{j+1/2}$ and $\Delta f_{j+3/2}$, that is, $\Delta f_{j+1/2} + \Delta^2 f_{j+1}/2$ as shown in Figure 1, we get the inequality

$$\frac{1}{6}(b_2 - 1) \le \frac{1}{2}, \quad \text{that is,} \quad 1 < b_2 \le 4. \quad (29)$$

We can also derive the same inequality from another case that $|\Delta^2 f_{j+1}| > b_2 |\Delta^2 f_j|$. We will take $b = b_2 = 4$ in the numerical examples mentioned below.

Equations (21) to (28) can be extended to the MUSCL-type approach[8].

Efficient algorithms

Setting $\theta = 1$ and $\Delta\xi_i = \text{const.} = \Delta\xi$, and using the first-order upstream differences, we can formally write the equations of delta-form implicit schemes (10) and (12) as

$$[I + \lambda \sum_i (\nabla_i A_i^+ + \Delta_i A_i^-)]\, q = R \quad (30)$$

where $\lambda = \Delta t/\Delta\xi$, and ∇_i and Δ_i are the backward- and forward-difference operators in ξ_i direction respectively. Applying the approximate-factorization method and the diagonalization of (8) to (30), we get

$$\begin{aligned} &R_1[I + \lambda(\Lambda_1^+ \nabla_1 + \Lambda_1^- \Delta_1)] M_1^{-1} [I + \lambda(\Lambda_2^+ \nabla_2 + \Lambda_2^- \Delta_2)] M_2^{-1} \\ &\quad \times [I + \lambda(\Lambda_3^+ \nabla_3 + \Lambda_3^- \Delta_3)] L_3 q = R \end{aligned} \quad (31)$$

where

$$\begin{aligned} A_i^{\pm} &= R_i \Lambda_i^{\pm} L_i, \qquad (i = 1, 2, 3) \\ M_1 &= L_2 R_1, \qquad M_2 = L_3 R_2, \end{aligned} \quad (32)$$

A_i^+ and A_i^- are the diagonal matrices composed of only positive and negative eigenvalues respectively.

$$\tilde{M}_1 = \tilde{L}_2\tilde{R}_1 =$$

$$\begin{bmatrix}
1 & 0 & 0 & 0 & 0 & 0 & 0 \\
0 & (1-h_{22}^{12}h_{11}^{21})/2 & -h_{22}^{12} & 0 & (1-h_{22}^{12}h_{11}^{21})/2 & 0 & 0 \\
0 & (h_{11}^{21}+\sqrt{h_{11}^{22}})/2 & 1 & 0 & (h_{11}^{21}-\sqrt{h_{11}^{22}})/2 & 0 & 0 \\
0 & (h_{11}^{31}-h_{22}^{32}h_{11}^{21})/2 & -h_{22}^{32} & 1 & (h_{11}^{31}-h_{22}^{32}h_{11}^{21})/2 & 0 & 0 \\
0 & (h_{11}^{21}-\sqrt{h_{11}^{22}})/2 & 1 & 0 & (h_{11}^{21}+\sqrt{h_{11}^{22}})/2 & 0 & 0 \\
0 & 0 & 0 & 0 & 0 & 1 & 0 \\
0 & 0 & 0 & 0 & 0 & 0 & 1
\end{bmatrix},$$

$$\tilde{M}_2 - \tilde{L}_3\tilde{R}_2 =$$

$$\begin{bmatrix}
1 & 0 & 0 & 0 & 0 & 0 & 0 \\
0 & 1 & (h_{22}^{12}-h_{23}^{13}h_{22}^{32})/2 & -h_{33}^{13} & (h_{22}^{12}-h_{33}^{13}h_{22}^{32})/2 & 0 & 0 \\
0 & 0 & (1-h_{33}^{23}h_{22}^{32})/2 & -h_{33}^{23} & (1-h_{33}^{23}h_{22}^{32})/2 & 0 & 0 \\
0 & 0 & (h_{22}^{32}+\sqrt{h_{22}^{33}})/2 & 1 & (h_{22}^{32}-\sqrt{h_{22}^{33}})/2 & 0 & 0 \\
0 & 0 & (h_{22}^{32}-\sqrt{h_{22}^{33}})/2 & 1 & (h_{22}^{32}+\sqrt{h_{22}^{33}})/2 & 0 & 0 \\
0 & 0 & 0 & 0 & 0 & 1 & 0 \\
0 & 0 & 0 & 0 & 0 & 0 & 1
\end{bmatrix}$$

$h_{\ell\ell}^{ij} = g_{ij}/g_{\ell\ell}$. Equation (31) is solved by dividing into the seven steps:

$$\begin{aligned}
&\textbf{(I)} \quad q^{(1)} = L_1 R \\
&\textbf{(II)} \quad [I + \lambda(\Lambda_1^+\nabla_1 + \Lambda_1^-\Delta_1)]q^{(2)} = q^{(1)} \\
&\textbf{(III)} \quad q^{(3)} = M_1 q^{(2)} \\
&\qquad \cdots\cdots
\end{aligned} \tag{33}$$

Thus, the three-dimensional flow problem of (30), that a system of linear equations with a (7×7) block tri-diagonal matrix is solved, is reduced to the three simple one-dimensional problems of (33), that seven systems of linear equations with a scalar tri-diagonal matrix are solved. However, for the large Courant number $C_i = \Delta t|\Lambda_i|/\Delta\xi$, since errors caused by this factorization increase markedly, the convergency of the solution deteriorates.

Equation (30) can be also rewritten by applying the recently developed LU-SGS algorithm[9,10] as

$$(D+L)D^{-1}(D+U)q = R \tag{34}$$

where

$$L = \lambda \sum_i (\nabla_i A_i^+ - A_i^+),$$
$$U = \lambda \sum_i (\Delta_i A_i^- + A_i^-),$$
$$D = I + \lambda \sum_i |A_i|. \tag{35}$$

Further, in order to simplify the algorithm, the matrix D is diagonalized by setting

$$A_i^{\pm} = \frac{1}{2}(A_i \pm \rho_i I) \qquad \text{and} \qquad |A_i| = A_i^+ - A_i^- = \rho_i I \tag{36}$$

where $\rho_i = 1.01 \times |\lambda_{i\,\max}|$, and $\lambda_{i\,\max}$ is the maximum eigenvalue of A_i. Equation (34) is solved dividing into the two steps:
(I) Sweep from left bottom grid point

$$q^* = D^{-1}(R - Lq^*) \tag{37}$$

(II) Sweep from right top grid point

$$q = q^* - D^{-1}Uq \tag{38}$$

The errors caused by the factorization of (34) to (38) are relatively small, even for the large Coulant number, and the convergency of the solution is considerably improved compared with (31) to (33).

On the other hand, in order to remove the errors caused by the diagonalization of (36) and further to improve the convergency of the solution, the matrix D is factorized as

$$D = R_3 \Sigma L_1, \tag{39}$$

where $\sum$ is the semi-diagonally dominant matrix as

$$\Sigma = L_3 R_1 + \lambda(L_3 R_1 |\Lambda_1| + M_2 |\Lambda_2| M_1 + |\Lambda_3| L_3 R_1). \tag{40}$$

Then (34) can be split into six steps, and the systems of linear equations with coefficient matrix $\sum$ can be solved easily by Gaussian elimination. This LU-SGS-GE algorithm is like the LU-SGS-DC algorithm[11] except for some differences in matrix forms of (9) and solution of the system of linear equations; the details will be presented in the near future.

The flux vectors $\hat{F}_i$ in *RHS* of (11) are expressed after linearization like (17) as

$$
\begin{aligned}
(\Delta \hat{F}_i^{\pm})_{j+1/2} &= (J\hat{\Lambda}_i^{\pm})_{\ell+1/2}\Delta q_{j+1/2} \\
&\quad - (J\lambda_{i1}^{\perp})_{\ell+1/2}\Delta q_{j+1/2} \\
&\quad + \left[\begin{pmatrix} J\lambda_{ia}^{+} \\ c\sqrt{g_{ii}} \end{pmatrix}_{\ell+1/2} \Delta P + \left(\frac{J\lambda_{ib}^{\perp}}{g_{ii}}\right)_{\ell+1/2} \Delta M_i \right](Q_{ai})_{\ell+1/2} \\
&\quad + \left[\left(\frac{J\lambda_{ia}^{+}}{c\sqrt{g_{ii}}}\right)_{\ell+1/2} \Delta M_i + \left(\frac{J\lambda_{ib}^{\pm}}{c^2}\right)_{\ell+1/2} \Delta P \right](Q_b)_{\ell+1/2} \\
&\qquad\qquad (i = 1, 2, 3\,;\ j = \ell - 1,\ \ell,\ \ell + 1)
\end{aligned}
\tag{41}
$$

where

$$
\begin{aligned}
&\lambda_{i1} = U_i\,, \quad \lambda_{i4} = U_i + c\sqrt{g_{ii}}\,, \quad \lambda_{i5} = U_i - c\sqrt{g_{ii}}\,, \\
&\lambda_{ia}^{\pm} = \frac{1}{2}(\lambda_{i4}^{\pm} - \lambda_{i5}^{\pm})\,, \quad \lambda_{ib}^{\pm} = \frac{1}{2}(\lambda_{i4}^{\pm} + \lambda_{i5}^{+}) - \lambda_{i1}^{\perp}\,,
\end{aligned}
\qquad (i = 1, 2, 3) \tag{42}
$$

$$
\begin{aligned}
\Delta P &= (\phi^2 \ \ -\tilde{\gamma}u \ \ -\tilde{\gamma}v \ \ -\tilde{\gamma}w \ \ \tilde{\gamma} \ \ 0 \ \ 0)_{\ell+1/2} \cdot \Delta q_{j+1/2}\,, \\
\Delta M_i &= (-U_i \ \ \xi_{i,1} \ \ \xi_{i,2} \ \ \xi_{i,3} \ \ 0 \ \ 0 \ \ 0)_{\ell+1/2} \cdot \Delta q_{j+1/2}\,, \quad (i = 1, 2, 3)
\end{aligned}
\tag{43}
$$

$$
q = \begin{bmatrix} \rho \\ \rho u \\ \rho v \\ \rho w \\ \rho E \\ \rho k \\ \rho \varepsilon \end{bmatrix}, \quad Q_{ai} = \begin{bmatrix} 0 \\ \xi_{i,1} \\ \xi_{i,2} \\ \xi_{i,3} \\ U_i \\ 0 \\ 0 \end{bmatrix}, \quad Q_b = \begin{bmatrix} 1 \\ u \\ v \\ w \\ H \\ k \\ \varepsilon \end{bmatrix}. \qquad (i = 1, 2, 3) \tag{44}
$$

We should say that the excellent computational results of compressible flows containing discontinuities can be obtained only by using such an exact linearization. The numerical flux in the MUSCL-type approach can be linearized in a similar manner[4].

Numerical examples

For the simple steady compressible flow having shock waves, the computational results by the Chakravarthy-Osher TVD scheme (15) and the fourth(fifth)-order version (19) in general do not differ greatly, and the differences between the previous method using the fourth-order corrections (25) to prevent new extremum points completely and the present method using the fourth-order corrections (27) to suppress new inflection points appear to be even fewer. However, for some complicated flows so that the diffusive effects are

decisive, the computational results, especially the distributions of fluid dynamic losses and turbulence correlations, are appreciably different by (25) and (27). In the computation of such flows, it is important to make use of the scheme which has very few truncation and inherited errors.

Here the computational results are shown of steady and unsteady two-dimensional transonic flows through a turbine cascade composed of VKI LS-59 blades, experimented by Kiock *et al.*[12]. Figure 2 shows the computational grid of modified H-type having 181×61 grid points and the magnification near the trailing edge of the blade. The distances from the wall to the neighbouring grid point y^+ are roughly less than one. The total temperature 290 K, the total pressure 0.964×10^5 Pa and the inlet flow angle 30 deg as the upstream boundary conditions, and the Mach number 0.99 as the downstream boundary condition are imposed. The turbulence intensity 2 per cent at the upstream boundary and the Reynolds number 8.5×10^5 in the downstream region are assumed.

Steady flows

The actual flow through this turbine cascade is an unsteady flow containing vortex streets from the trailing edge of the blades. However, if calculation of the cascade flow problem is performed using the steady flow scheme of (10), then the solution converges almost uniformly for an appropriate range of Courant numbers and a steady flow solution can be obtained. Here, in order to calculate the solution efficiently, the local time-step technique, widely-used in steady flow calculation, is introduced, in which the local time step Δt as

$$\Delta t = \min\left(\frac{\Delta\xi}{|U_1| + c\sqrt{g_{11}}}, \frac{\Delta\xi}{|U_2| + c\sqrt{g_{22}}}\right) CFL$$

is used. Figure 3 shows the convergence histories of the solutions (the root-mean-squared residuals of the continuity equation) obtained for the relatively large Courant number $CFL = 45$, by the previous method using (25) and the present method using (27). The computations in the early stage were performed under the laminar flow condition and at $CFL = 1$. It is found from this figure that the solution by the present method of (27) converges better than the previous method of (25). The cause can be explained easily by the isentropic Mach number distributions on the blade surfaces. Although the Mach number distribution of (27) converges, the Mach number distribution of (25) oscillates in time and the typical distribution at a time step contains some numerical disturbances, as shown in Figure 4. The solution of (27) for $CFL = 100$ converged more rapidly, but the solution of (25) for $CFL = 60$ diverged. On the other hand, if CFL is taken as less than 2 in the calculation using (25), then the residuals can be reduced to a sufficiently low level, although, of course, the computational efficiency deteriorates.

Unsteady flows

The unsteady solution of this turbine cascade flow problem can be obtained by using the unsteady flow scheme of (12) with the higher-order scheme (21). The computational grid and the boundary conditions are same as the steady flow. The computation starts from the steady flow solution. The same time interval $\Delta t = 0.001$ is used throughout the flow field. Then, the maximum value of CFL_1

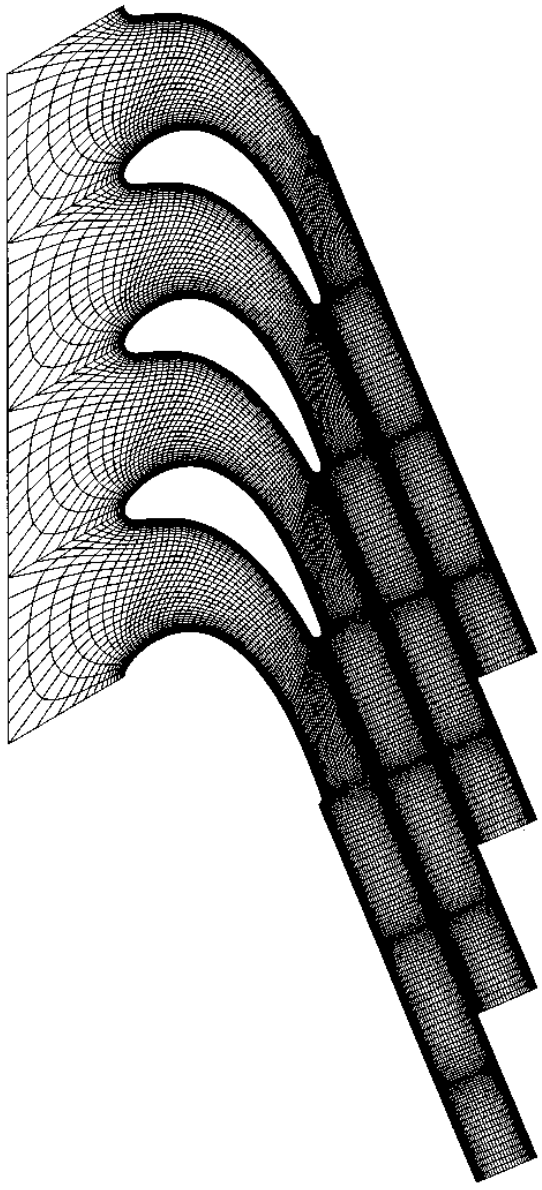

Figure 2a.
Computational grid for turbine cascade with VKI LS-59 blades – whole view

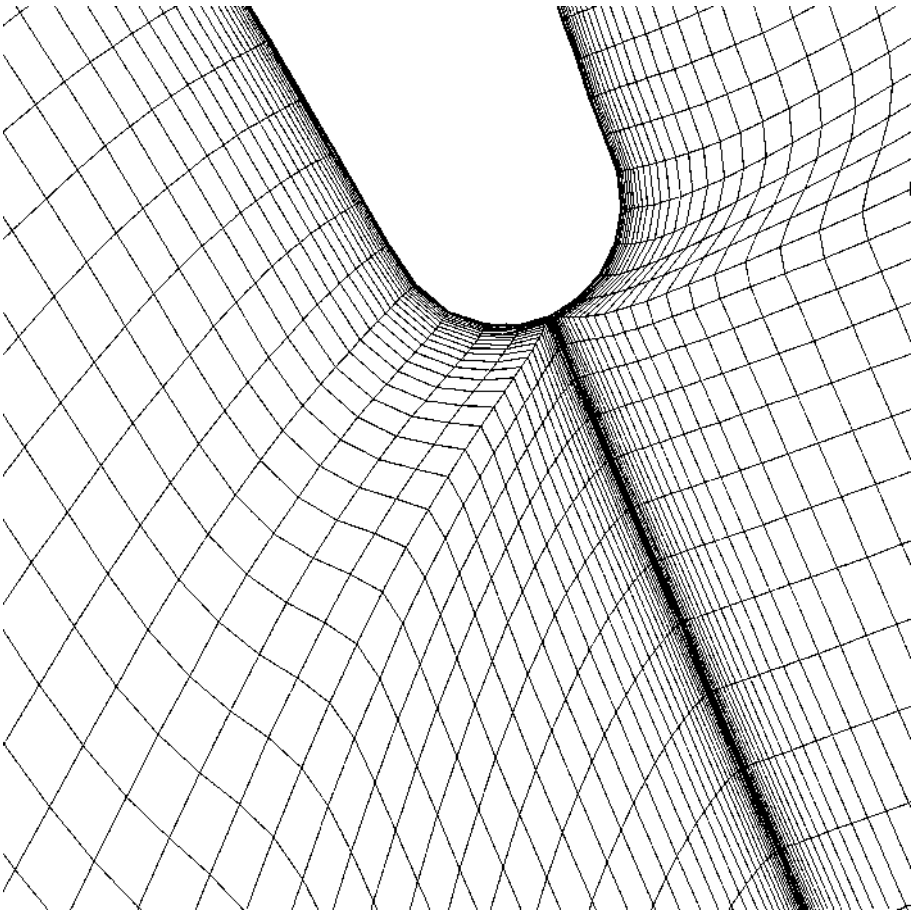

Figure 2b.
Computational grid for turbine cascade with VKI LS-59 blades – near trailing edge of blade

$\equiv \Delta t\,(|U_1| + c\sqrt{g_{11}})/\Delta\xi$ is very small, but the maximum value of $CFL_2 \equiv \Delta t\,(|U_2| + c\sqrt{g_{22}})/\Delta\xi$ becomes about 20 on the solid wall. The iterations of (12) are carried out four times at each time step. Figure 5 shows the time variations of residuals. The residual values in the case of (27) are one unit smaller than those of (25). Therefore, using (27) will make it possible to obtain accurate solutions within a relatively small number of iterations. The time-averaged isentropic Mach number distributions on the blade surfaces almost coincide with the experimental data as shown in Figure 6, different from the steady flow.

Finally, the more subtle differences in some of the numerical results of this unsteady turbine cascade flow, calculated by the previous method using (25) and the present method using (27), are discussed. Figure 7 shows a comparison of the contours of velocity component u. Both the figures reveal the existence of vortex streets, clear left-running shock waves and vortex/shock-wave

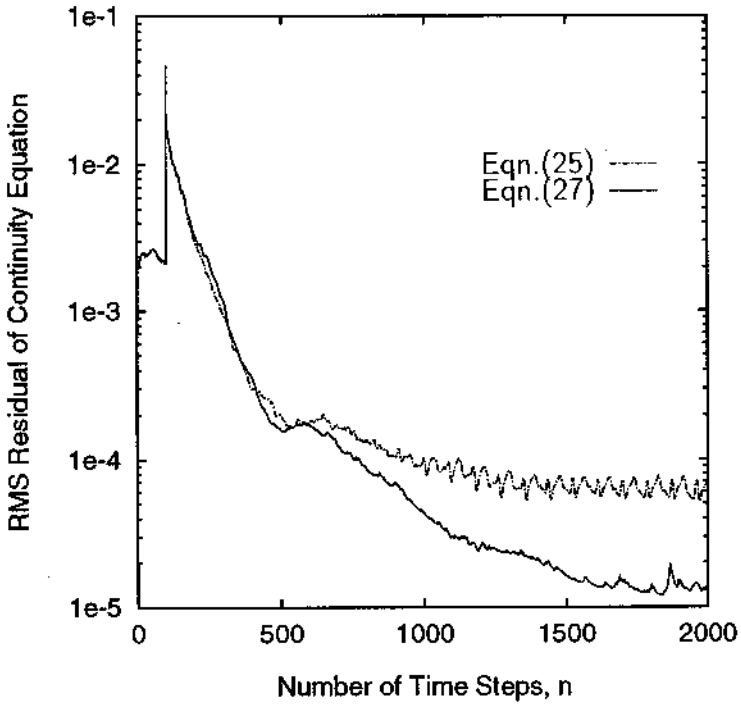

Figure 3.
A comparison of convergence histories for steady flow

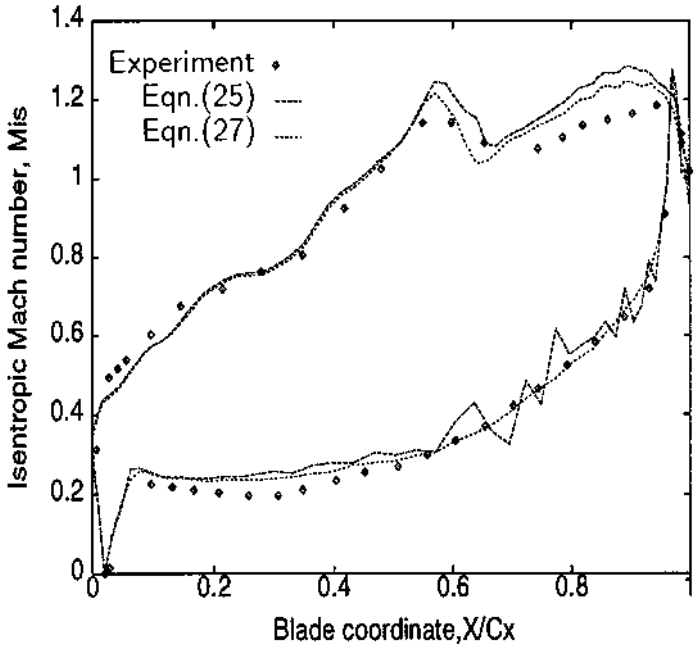

Figure 4.
Typical isentropic Mach number distributions on blade surfaces for steady flow

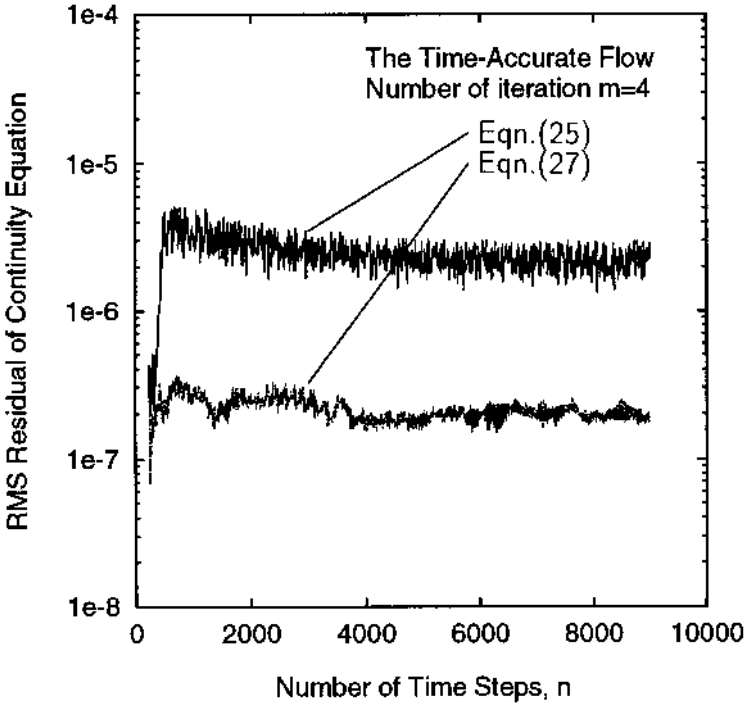

Figure 5.
A comparison of time-variations of residuals for unsteady flow

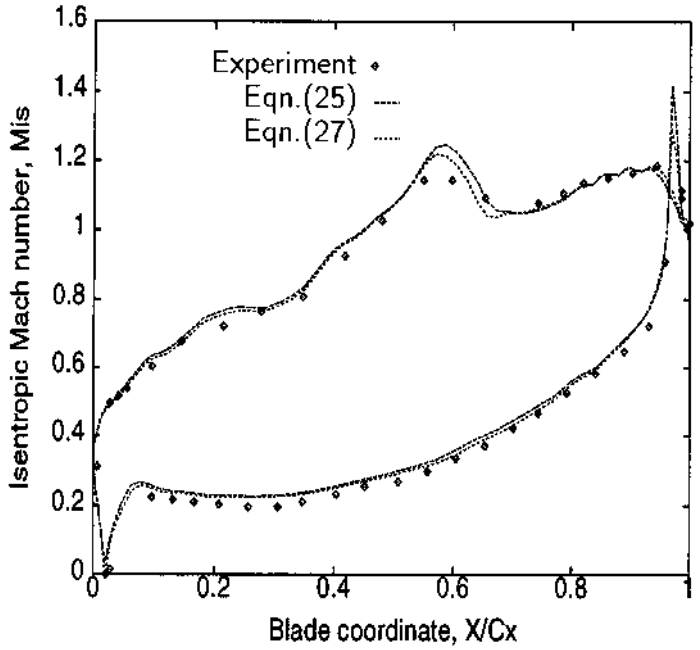

Figure 6.
Time-averaged isentropic Mach number distribution on blade surfaces for unsteady flow

interactions. Further, it can be observed that the space between the neighbouring vortices of (27) is a little shorter than the space of (25), that is, the Strouhal number of (27) is greater than (25), and that the behaviours of right-running shock waves are somewhat different. The values of stagnation

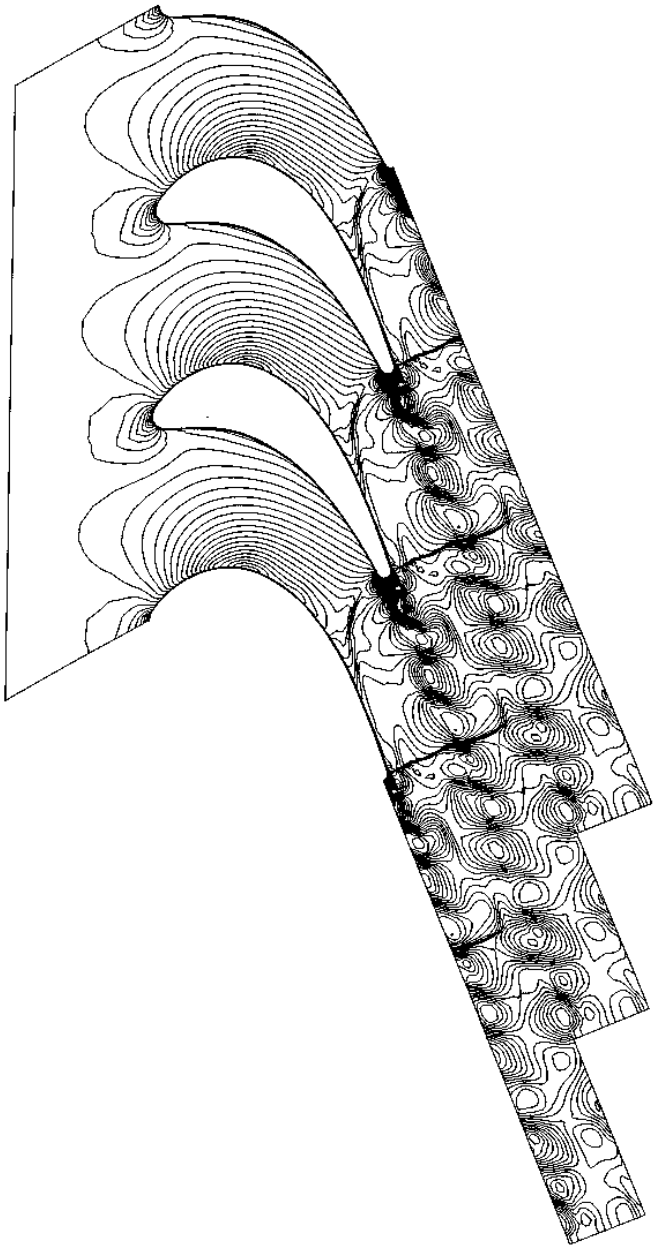

Figure 7a.
Instantaneous contours of velocity component *u*: previous method using (25)

enthalpy H are constant in the isentropic flow without diffusion, and therefore the contours of H in Figure 8 indicate the fluid dynamic losses; and the contours of eddy viscosity μ_t in Figure 9 show the turbulence of the flow. It is found from these figures that the values of u, H and μ_t calculated by the previous and

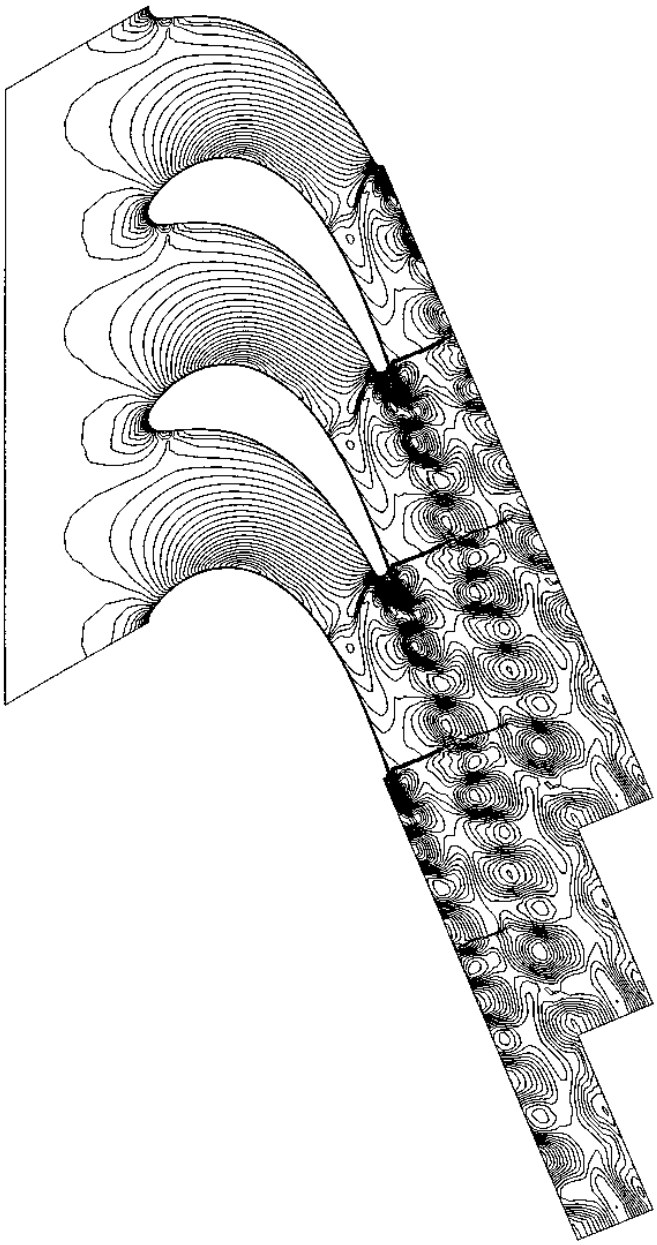

Figure 7b. Instantaneous contours of velocity component u: present method using (27)

present methods are appreciably different. However, the estimation of these differences is not yet ready for disclosure. Although it is not always easy to determine the loss coefficient and outlet flow angle of the transonic turbine cascade flows numerically, the calculated results of these quantities by the

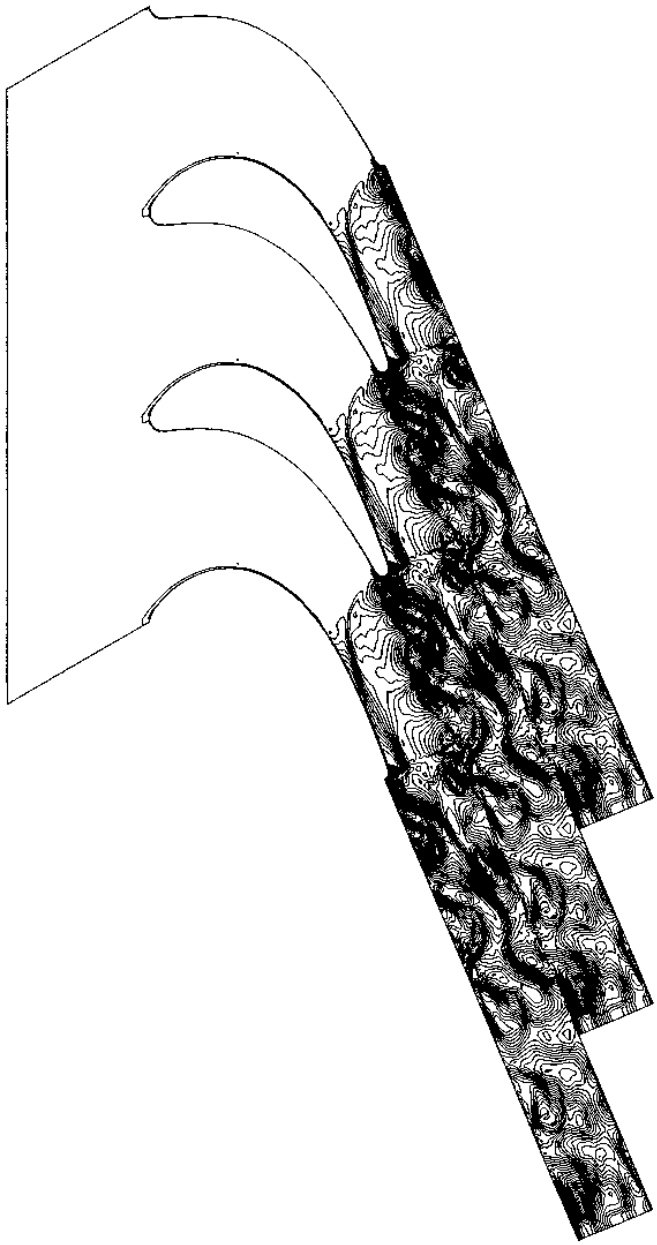

Figure 8a.
Instantaneous contours of stagnation enthalpy *H*: previous method using (25)

present method agree very well with the experimental data[13]. Further, it can be seen that the convergency of the solution is improved not only by the stabilization measure of (27) and the LU-SGS-GE algorithm of (39) and (40) but also by the exact linearization of (41) to (44).

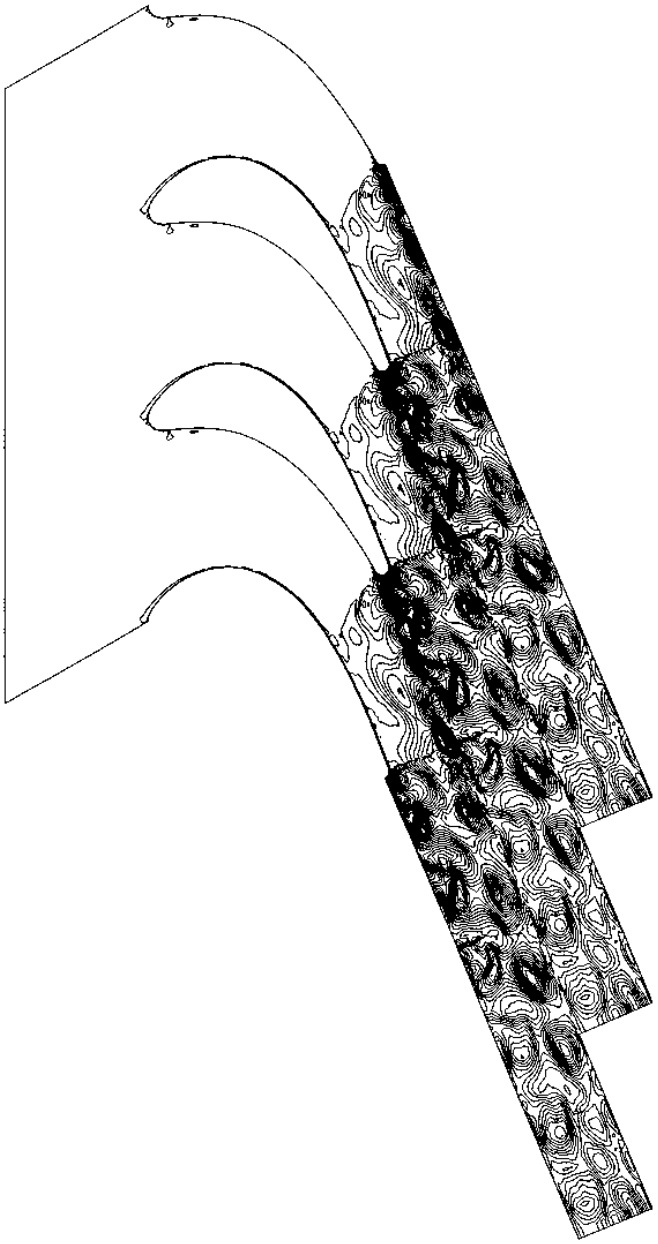

Figure 8b.
Instantaneous contours of stagnation enthalpy *H*: present method using (27)

Concluding remarks

Numerical instabilities occurring in the process of numerical computation first appear as inflection points, which then grow gradually and finally form extremum points. Although the stabilization of the existing second-order TVD

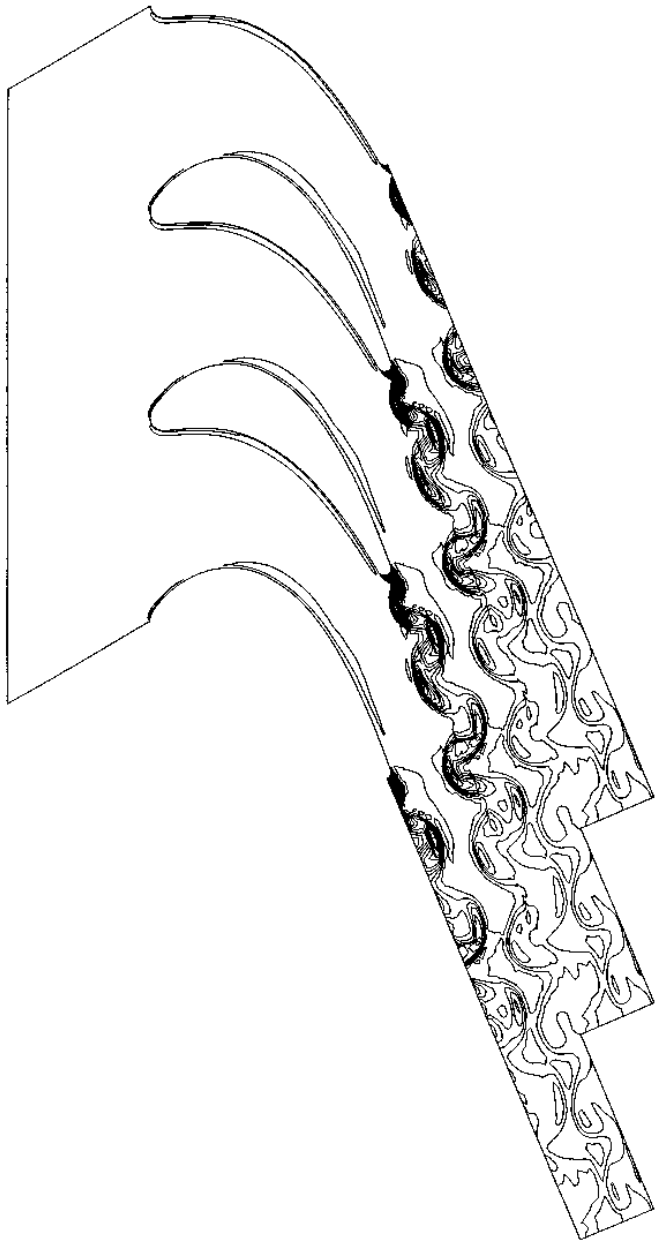

Figure 9a.
Instantaneous contours of eddy viscosity μ_t: previous method using (25)

schemes has been performed so that the extremum points do not occur, if the stabilization measure can be taken in the stage of occurrence of the inflection points, the schemes would be better. In the existing Chakravarthy-Osher TVD scheme, the values of the second(third)-order correction terms are restricted by

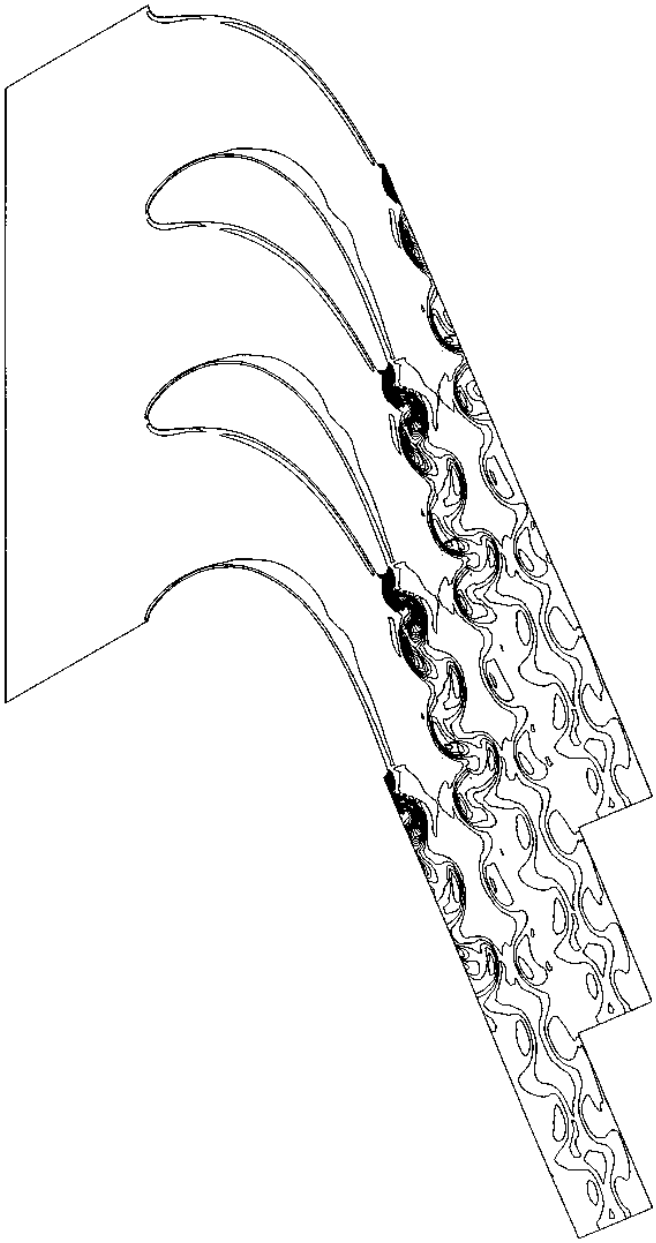

Figure 9b.
Instantaneous contours of eddy viscosity μ_t: present method using (27)

operating the limiter functions to the slopes $\Delta u_{j+1/2}$, in order to prevent the occurrence of new extremum points. In the present scheme, in addition to this restriction, the values of the fourth(fifth)-order correction terms are restricted by operating another limiter function to the curvatures $\Delta^2 u_j$, in order to suppress the occurrence of new inflection points. However, not all the inflection points are suppressed, owing to numerical instabilities, only the inflection points caused by the fourth(fifth)-order correction terms. In order to suppress all the inflection points, it may be necessary to restrict appropriately not only the fourth(fifth)-order correction terms but also the second(third)-order correction terms. This remains a problem for future investigation.

References

1. Chakravarthy, S.R. and Osher, S., "A new class of high accuracy TVD schemes for hyperbolic conservation laws", *AIAA Paper 85-0363*, AIAA, New York, NY, 1985.
2. Davis, S.F., "TVD finite difference schemes and artificial viscosity", *ICASE Report 84-20*, 1984.
3. Roe, P.L., "Generalized formulation of TVD Lax-Wendroff schemes", *ICASE Report 84-53*, 1984.
4. Yamamoto, S. and Daiguji, H., "Higher-order-accurate upwind schemes for solving the compressible Euler and Navier-Stokes equations", *Comp. Fluids*, Vol. 22, 1993, pp. 259-70.
5. Yamamoto, S., Takahashi, A. and Daiguji, H., "Higher-order numerical simulation of unsteady shock/vortex interactions", *AIAA Paper 94-2305*, AIAA, New York, NY, 1994.
6. Daiguji, H. and Yamamoto, S., "An implicit time marching method for solving the 3-D compressible Navier-Stokes equations", *Lecture Notes in Physics*, Vol. 323, Springer-Verlag, Berlin, 1988, pp. 210-14.
7. Chien, K.-Y., "Prediction of channel and boundary layer flows with a low Reynolds number turbulence model", *AIAA Journal*, Vol. 20, 1982, pp. 33-8.
8. Hirsch, C., *Numerical Computation of Internal and External Flows*, Vol. 2, John Wiley & Sons, Chichester, 1990, pp. 495-505.
9. Jameson, A. and Yoon, S., "Lower-upper implicit schemes with multi grids for the Euler equations", *AIAA Journal*, Vol. 25, 1987, pp. 929-35.
10. Yoon, S. and Kwak, D., "Implicit Navier-Stokes solver for three-dimensional compressible flows", *AIAA Journal*, Vol. 30, 1992, pp. 2653-9.
11. Yuan, X. and Daiguji, H., "A new LU-type implicit scheme for three-dimensional compressible Navier-Stokes equations", *6th International Symposium on Computational Fluid Dynamics*, Lake Tahoe, NV, Vol. III, 1995, pp. 1473-8.
12. Kiock, R., Lehthaus, F., Baines, N.C. and Sieverding, C.H., "The transonic flow through a plane turbine cascade as measured in four European wind tunnels", *Trans. ASME, J. Engng. Gas Turbine and Power*, Vol. 108, 1986, pp. 277-85.
13. Yuan, X. and Daiguji H., "Development of efficient Navier-Stokes solver for application to general large-scale turbine blade designs", *Proceedings of CSPE-JSME-ASME International Conference on Power Engineering-95*, Shanghai, Vol. 2, 1995, pp. 573-83.